

3D-Aware Semantic-Guided Generative Model for Human Synthesis

Jichao Zhang¹, Enver Sangineto¹, Hao Tang², Aliaksandr Siarohin¹, Zhun Zhong¹
Nicu Sebe¹, Wei Wang¹

¹ Multimedia and Human Understanding Group (MHUG), University of Trento

² Computer Vision Lab, ETH Zurich

Abstract

Generative Neural Radiance Field (GNeRF) models, which extract implicit 3D representations from 2D images, have recently been shown to produce realistic images representing rigid objects, such as human faces or cars. However, they usually struggle to generate high-quality images representing non-rigid objects, such as the human body, which is of a great interest for many computer graphics applications. This paper proposes a 3D-aware Semantic-Guided Generative Model (3D-SGAN) for human image synthesis, which integrates a GNeRF and a texture generator. The former learns an implicit 3D representation of the human body and outputs a set of 2D semantic segmentation masks. The latter transforms these semantic masks into a real image, adding a realistic texture to the human appearance. Without requiring additional 3D information, our model can learn 3D human representations with a photo-realistic controllable generation. Our experiments on the DeepFashion dataset show that 3D-SGAN significantly outperforms the most recent baselines.

1. Introduction

Recent deep generative models can generate and manipulate high-quality images. Specifically, Generative Adversarial Networks (GANs) [12], have been applied to different tasks, such as image-to-image translation [73, 9, 22], portrait editing [2, 61, 67, 62], and semantic image synthesis [50], to mention a few. However, most state-of-the-art GAN models [16, 25, 28, 29, 26, 17, 27] are trained using 2D images, operate in the 2D domain and ignore the 3D nature of the world. Thus, they often struggle to disentangle the underlying 3D factors.

Recently, different 3D-aware generative models [46, 47, 69] have been proposed to solve this problem. Since most of these methods do not need 3D annotations, they can cre-



Figure 1: A qualitative comparison between different human image generation methods: GRAF [60], pi-GAN [7], GIRAFFE [49] and 3D-SGAN (ours).

ate 3D content while reducing the hardware costs of common computer graphics alternatives. Differently from generating 3D untextured shapes [69, 11], some of these methods [74, 8, 46, 35, 47] focus on 3D-aware realistic image generation and controllability. Generally speaking, these models mimic the traditional computer graphics rendering pipeline: they first model the 3D structure, then they use a (differentiable) projection module to project the 3D structure into 2D images. The latter may be a depth map [8], a sketch [74] or a feature map [46] which is finally mapped into the real image by a rendering module. During training, some methods require 3D data [74, 8], and some [46, 35, 47] can learn a 3D representation directly from raw images.

An important class of *implicit* 3D representations is composed of Neural Radiance Fields (NeRFs), which can generate high-quality novel views of complex scenes [44, 23, 10, 52, 51, 53, 7]. Generative NeRFs (GNeRFs) combine NeRFs with GANs in order to condition the generation process with a latent code governing the object’s appearance or shape [60, 7, 49]. However, these methods [60, 7, 49] focus on relatively simple and “rigid” objects, such as cars and faces, and they usually struggle to generate non-rigid objects such as the human body (e.g., see Fig. 1). This

is likely due to the fact that the human body appearance is highly variable because of both its articulated poses and the variability of the clothes texture, being these two factors entangled with each other. Thus, adversarially learning the data distribution modeling all those factors, is an hard task, especially when the training set is relatively small.

To mitigate this problem, we propose to *split* the human generation process in two separate steps and use intermediate segmentation masks as the bridge of these two stages. Specifically, our 3D-aware Semantic-Guided Generative model (3D-SGAN) is composed of two generators: a GNeRF model and a texture generator. The GNeRF model learns the 3D structure of the human body and produces a semantic segmentation of the main body components, which is largely invariant to the surface texture. The texture generator translates the previous segmentation output into a photo-realistic image. To control the texture style, a Variational AutoEncoder (VAE [32]) is used to modulate the final decoding process. We empirically show that splitting the human generation process into these two stages brings the following three advantages. First, the GNeRF model is able to learn the intrinsic 3D geometry of the human body, even when trained with a small dataset (e.g., DeepFashion [37]). Second, the texture generator can successfully translate semantic information into a textured object. Third, both generators can be controlled by explicitly varying their respective conditioning latent codes. Moreover, we propose two consistency losses to further disentangle the latent codes representing the garment type (which we call “semantic” code) and the human pose. Experiments conducted on the DeepFashion dataset [37] show that 3D-SGAN can generate high-quality person images significantly outperforming state-of-the-art approaches.

In summary, the main contributions of this work are:

- 1) We propose 3D-SGAN, a 3D-aware semantic-guided generative model, which integrates a GNeRF with a VAE-conditioned texture generator for human synthesis.
- 2) We propose two consistency losses to increase the disentanglement between semantic information (e.g., garment type) and the human pose.
- 3) We show that 3D-SGAN generates high-quality human images, significantly outperforming the previous controllable state-of-the-art methods.

2. Related work

3D-aware image synthesis is based on generative models which incorporate a 3D scene representation. This allows rendering photo-realistic images from different viewpoints. Early methods use GAN-based architectures for building 3D voxel [69, 11, 39, 19] or mesh [55, 18] representations. However, they mostly focus on learning un-

textured 3D structures. More recently, different methods learn textured representations directly from 2D images [68, 74, 46, 60, 10, 48, 49]. The resulting controllable 3D scene representation can be used for image synthesis. Some of these methods [74, 8] require extra 3D data for disentangling shape from texture. The main idea is to generate an internal 3D shape and then project this shape into 2D sketches [74] or depth maps [8], which are finally rendered in a realistic image. Other methods are directly trained on 2D images without using 3D data [46, 60, 47, 49]. For instance, inspired by StyleGANv2 [29], Thu et al. [46] propose HoloGAN, which predicts 3D abstract features using 3D convolutions, and then projects these features into a 2D representation which is finally decoded into an image. However, the learnable projection function, e.g., the decoder, results in entangled representations, thus the view-consistency of the generated images is degraded. On the other hand, Katja et al. [60] use a NeRF to represent the 3D scene and a volume rendering technique to render the final image. However, this model works at relatively low image resolutions and it is restricted to single-object scenes. To tackle these issues, some works propose object-aware scene representations. For example, Liao et al. [35] combine a 2D generator and a projection module with a 3D generator which outputs multiple abstract 3D primitives. Every stage in this model outputs multiple terms to separately represent each object. Instead of abstract 3D primitives, Phuoc et al. [47] use a voxel feature grid as the 3D representation, but their method fails to generate consistent images at high-resolution. Michael et al. [49] recently introduced GIRAFFE, a multiple-object scene representation based on NeRFs and an object composition operator. GIRAFFE is the state-of-the-art 3D-aware approach for both single and multiple object generation tasks.

While previous methods achieve impressive rigid-object generation and manipulation results, they usually struggle to deal with non-rigid objects with complex pose and texture variations. From the application point of view, an important example of non-rigid object is the human body.

GANs for human generation. GANs [12] have attracted a lot of attention in recent years because of their high quality generation results. They have been widely used for different object categories, such as, for instance, faces [30, 25, 28, 6], cars [30, 28, 60, 47], and churches [49]. However, GANs still struggle to produce high-quality human person images, because of the complex pose variations. Very recently, Sarkar et al. [58] proposed a VAE-GAN model for the pose transfer and the part sampling tasks. In more detail, this model extracts an UV texture map from the input image using DensePose [3], and then encodes the texture into a Gaussian distribution. Then, it samples from this distribution and warps the sample into the target pose space. Finally, the warped latent code is used as input to the de-

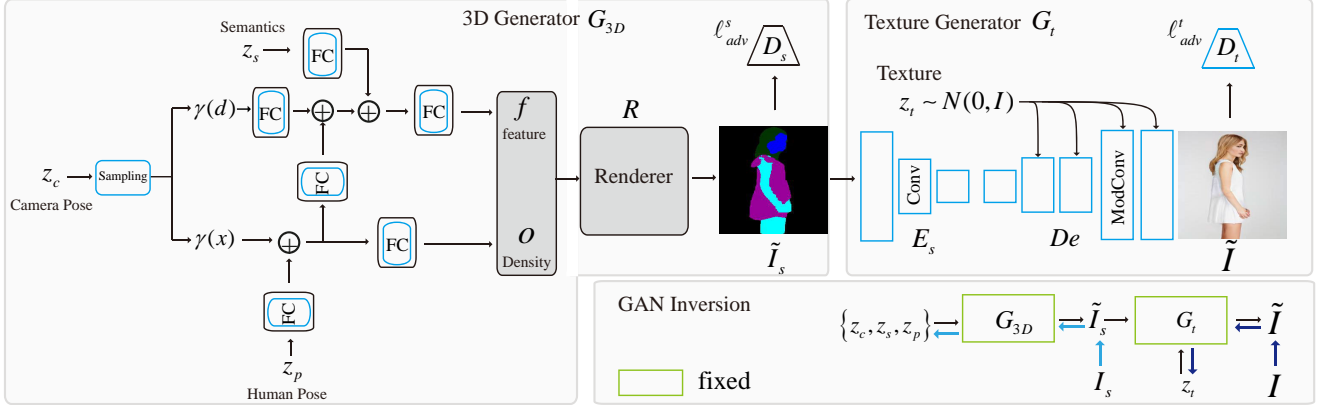


Figure 2: An overview of the proposed 3D-SGAN architecture, composed of two main generators. G_{3D} (on the left) follows a GNeRF structure, with a NeRF kernel used to represent implicit 3D information, latent codes governing different appearance variations and a discriminator (D_s) which is used for adversarial training. The output of G_{3D} is the semantic masks \tilde{I}_s (middle). The second generator (G_t , right) translates the semantic masks into a photo-realistic image \tilde{I} . Also G_t is trained adversarially (see top right, the second discriminator D_t). The human generation process can be controlled by interpolating different latent codes: the semantics code z_s , the pose code z_p , the camera code z_c , and the texture code z_t . The bottom of the figure shows the GAN inversion scheme.

coder. Compared to Sarkar et al. [58], our method does not use an SMPL nor DensePose to extract the point correspondences as supervised information. Despite that, 3D-SGAN can learn 3D representations of the human body and control the generation process (e.g., by changing the input camera parameters).

Grigorev et al. [13] propose a StylePeople framework which is based on a full-body human avatar, which combines StyleGANv2 [29] with *neural dressing*. StyleGANv2 [29] samples neural textures, and these textures are superimposed on the meshes of an SMPL. The textured meshes are finally rendered into an image. In contrast, our 3D-SGAN can perform semantic disentanglement and manipulation using semantic code.

Pose transfer aims to synthesize person images in a novel view or in a new pose. This is a very challenging task, since it requires very complicated spatial transformations to account for different poses. Most works in this field can be categorized by the way in which the human pose is represented. Early works are based on keypoints [41, 63, 75, 54, 66, 42, 43, 21, 5, 40, 24, 65, 64, 72, 56, 70]. More recent methods [14, 45, 59, 57, 36] use correspondences between pixel location in 2D images and points in SMPL [38] model. These correspondences are usually estimated using DensePose [15]. However, these approaches usually struggle to simultaneously provide a realistic and a 3D controllable person generation. In contrast, 3D-SGAN is a 3D controllable person generation method which does not require SMPL models or 3D supervision. Importantly, our method is an unconditioned generative model which allows random sampling from a learned marginal distribution of the data.

3. Preliminaries

NeRF [44] is an implicit model which represents a 3D scene using the weights of a multilayer perceptron (MLP). This MLP (h) takes as input a 3D coordinate $\mathbf{x} \in \mathbb{R}^3$ and a view direction $\mathbf{d} \in \mathbb{R}^2$, and outputs the density (or “opacity”, o) and the view-dependent RGB color value \mathbf{c} :

$$(\mathbf{c}, o) = h(\gamma(\mathbf{x}), \gamma(\mathbf{d})), \quad (1)$$

where γ is a positional encoding function. On the other hand, Generative NeRF (GNeRF) [60] is a conditional NeRF which additionally takes as inputs latent codes \mathbf{z}_g and \mathbf{z}_a , respectively representing the geometric shape and the appearance, and which are drawn from a priori distributions. GNeRFs are trained using an adversarial approach. In GIRAFFE [49], the color value (\mathbf{c} in Eq. 1) is replaced by an intermediate feature vector \mathbf{f} :

$$(\mathbf{f}, o) = h(\gamma(\mathbf{x}), \gamma(\mathbf{d}), \mathbf{z}_g, \mathbf{z}_a). \quad (2)$$

\mathbf{f} is mapped into a photo-realistic image using a volume and neural rendering module R and fed to a discriminator (more details in [60, 49]).

Our 3D generator (see Sec. 4) is inspired by GIRAFFE [49]. However, it learns to produce a segmentation image, a simpler task with respect to directly generating a photo-realistic image (see Sec. 1).

4. The proposed 3D-SGAN

Fig. 2 shows the proposed 3D-SGAN architecture, which has two main modules: a 3D-based segmentation mask generator and a texture generator. The former (G_{3D}) generates semantic segmentation masks of the human body which correspond to the main body parts and depend on the type of

clothes, the camera viewpoint and the human pose. On the other hand, the texture generator (G_t) takes as input these segmentation masks and translates them into a photo-realistic image, adding a texture style randomly drawn from a pre-learned marginal distribution. The two modules are trained separately, and we provide below the details of both the proposed architectures and the training method.

4.1. 3D generator for semantic mask rendering

Given a set of 2D human image samples $\{I^i\}_{i=1}^N$, we first use an off-the-shelf human parsing tool [4] to obtain the corresponding ground-truth semantic segmentation masks $\{I_s^i\}_{i=1}^N$. Using $T = \{(I^i, I_s^i)\}_{i=1}^N$ as our training set, the goal is to train a two-step generative model:

$$\tilde{I} = G(z_c, z_s, z_p, z_t) = G_t(G_{3D}(z_c, z_s, z_p), z_t), \quad (3)$$

where \tilde{I} is the photo-realistic generated image. The latent codes $z_c \sim P_c$ (see Sec.6), $z_s \sim \mathcal{N}(0, \mathbf{I})$, $z_p \sim \mathcal{N}(0, \mathbf{I})$, and $z_t \sim \mathcal{N}(0, \mathbf{I})$ represent, respectively: the camera viewpoint, the semantics (i.e., the garment type), the human body pose and the human texture.

The structure of our 3D Generator G_{3D} is inspired by GIRAFFE [49] (Sec. 3). However, differently from [60, 49], which learn to generate a textured object, in our case, h learns to generate a semantically segmented image. Specifically, we use a latent semantic code (z_s) to condition the final segmentation output on the type of garment. As shown in Fig. 2, z_s does not influence the opacity generation branch, and it is injected into the direction-dependent branch, which finally outputs a feature vector \mathbf{f} , representing a point-wise semantic content. Formally, we have:

$$(\mathbf{f}, o) = h(\gamma(\mathbf{x}), \gamma(\mathbf{d}), z_c, z_s, z_p). \quad (4)$$

Following [60, 49], we generate a set of pairs $\{(\mathbf{f}, o)\}$ which are finally projected into the 2D plane using a rendering module R [44, 49] (see Sec. 3), and represented by the segmentation masks \tilde{I}_s . Specifically, \tilde{I}_s is a tensor composed of n_s channels, where each channel represents a segmentation mask of the same spatial resolution of the real images in T (Fig. 2).

G_{3D} is trained jointly with a discriminator D_s , which learns to discriminate between real (I_s) and fake (\tilde{I}_s) segmentation masks (more details in Sec. 4.4).

4.2. VAE-conditioned texture generator

The goal of our texture generator G_t is twofold: (1) mapping the segmentation masks \tilde{I}_s generated by G_{3D} into a textured human image and (2) learning a marginal distribution of the human texture using the dataset T . The latter is obtained using a Variational AutoEncoder (VAE [32]) framework, which we use to learn how to *modulate* the texture style of the decoder. Specifically, as shown in Fig. 3,

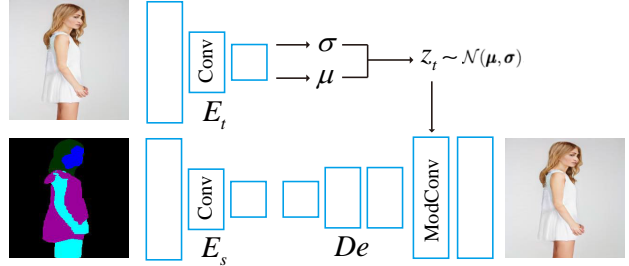


Figure 3: The proposed VAE-conditioned texture generator. ModConv stands for “Modulated Convolution” [29].

G_t is composed of a semantic encoder E_s , a texture encoder E_t , and a decoder De . De is based on a StyleGANv2 architecture [29], in which a style code is used to “demodulate” the weights of each convolutional layer. We modify this architecture using a variational approach, in which the style code, *at inference time*, is extracted from a learned marginal distribution. In more detail, given a segmentation tensor I_s , we use E_s to extract the semantic content. This semantic content is decoded into the final image using De and a texture code z_t . The latter is sampled using the VAE encoder E_t , which converts a real input image I into a latent-space normal distribution ($\mathcal{N}(\boldsymbol{\mu}, \boldsymbol{\sigma})$), from which z_t is randomly chosen:

$$(\boldsymbol{\mu}, \boldsymbol{\sigma}) = E_t(I), z_t \sim \mathcal{N}(\boldsymbol{\mu}, \boldsymbol{\sigma}), \tilde{I} = De(E_s(I_s), z_t). \quad (5)$$

G_t is trained using the pairs in T . Specifically, given a pair of samples (I^i, I_s^i) , we use an adversarial loss ℓ_{adv}^t jointly with a reconstruction loss ℓ_r , and a standard Kullback-Leibler divergence loss (ℓ_{kl}) [32]:

$$\ell_r = \|G_t(I_s^i, z_t) - I^i\|_1, \ell_{kl} = \mathcal{D}_{kl}(z_t \| \mathcal{N}(\mathbf{0}, \mathbf{I})), \quad (6)$$

where \mathcal{D}_{kl} is the Kullback-Leibler divergence. Note that, in the reconstruction process, G_t cannot ignore the segmentation tensor (I_s^i) and its corresponding encoder E_s . In fact, the information extracted from the real image I , and encoded using E_t , is not enough for the decoder to represent the image content, since z_t is used only as a style modulator in De .

4.3. Consistency losses for semantic and pose disentanglement

In G_{3D} , the opacity value (o), computed by h , does not depend on the latent code z_s . Despite that, we have empirically observed that the semantics (z_s) and the pose (z_p) representations are highly entangled. For this reason, we propose two self-supervised consistency losses to further disentangle the semantic and the pose factors.

Silhouette-based geometric consistency. This loss is based on the idea that two different segmentation masks, produced using two different semantic codes z_{s1} and z_{s2} ,

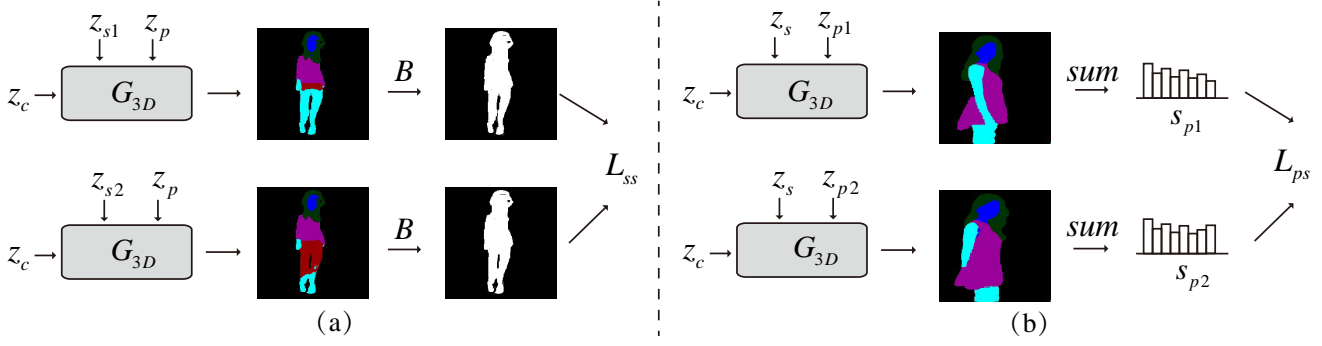


Figure 4: A schematic representation of the proposed consistency losses. (a) The Silhouette-based geometric consistency loss ℓ_{ss} . (b) The pose consistency loss ℓ_{ps} .

but keeping fixed the pose and the camera codes, should result in a same overall silhouette (see Fig. 4 (a)). Formally, the proposed geometric consistency loss ℓ_{ss} is defined as:

$$\ell_{ss} = \|B(G_{3D}(z_c, z_{s1}, z_p)) - B(G_{3D}(z_c, z_{s2}, z_p))\|_1, \quad (7)$$

where $B(\tilde{I}_s)$ maps the segmentation masks \tilde{I}_s into a binary silhouette image.

Pose-based semantic consistency. Analogously to ℓ_{ss} , the proposed pose-based semantic consistency loss is based on the idea that two different pose codes should produce a similar semantic content. However, as shown in Fig. 4 (b), despite the body being partitioned in similar semantic segments (e.g., because the clothes have not changed), when the human pose changes, the overall spatial layout of these segments can also change (e.g., see the two different arm positions in Fig. 4 (b)). For this reason, we formulate a semantic consistency loss (ℓ_{ps}) which is spatial-invariant, and it is based on the channel-by-channel comparison of two segmentation masks. In more detail, given two different pose codes z_{p1} and z_{p2} , and fixing the semantic code and the camera code, we first produce two corresponding segmentation tensors \tilde{I}_s^1 and \tilde{I}_s^2 . Then, for each tensor and each channel, we sum all the channel-specific mask values over the spatial dimension and we get two spatial invariant vectors $\mathbf{s}_{p1}, \mathbf{s}_{p2} \in \mathbb{R}^{n_s}$. Finally, ℓ_{ps} is given by:

$$\ell_{ps} = \sum_{i=1}^{n_s} [\max(\frac{|\mathbf{s}_{p1}[i] - \mathbf{s}_{p2}[i]|}{\mathbf{s}_{p1}[i] + \epsilon}, \rho) - \rho], \quad (8)$$

where $\mathbf{s}[i]$ is the i -th channel value of vector \mathbf{s} , ϵ is a small value used for numerical stability, and ρ is a margin representing the tolerable channel-wise difference.

4.4. Training and inference

G_{3D} is trained using an adversarial loss (ℓ_{adv}^s) jointly with the two consistency losses presented in Sec. 4.3:

$$\ell_{3D} = \ell_{adv}^s + \lambda_1 \ell_{ss} + \lambda_2 \ell_{ps}, \quad (9)$$

where λ_1 and λ_2 are hyper-parameters controlling the contribution of each loss term.

G_t is trained using a variational-adversarial approach (VAE-GAN [34]), with the overall objective function (ℓ_{tr}):

$$\ell_{tr} = \ell_{adv}^t + \lambda_3 \ell_r + \lambda_4 \ell_{kl}, \quad (10)$$

where λ_3 and λ_4 are hyper-parameters.

G_{3D} and G_t are trained separately. However, at inference time, the tensor \tilde{I}_s , generated by G_{3D} , is fed to G_t , along with a texture code z_t , randomly drawn from a standard normal distribution:

$$z_t \sim \mathcal{N}(\mathbf{0}, \mathbf{I}), \tilde{I} = D_e(E_s(\tilde{I}_s), z_t). \quad (11)$$

5. Real image editing using GAN inversion

Variational method of Fig. 3 can not completely reconstruct the input image. For real image editing, we use a GAN inversion technique [1] to optimize the values of latent codes corresponding to a real input image I . Since we have two separate generators (G_{3D} and G_t), the optimization process is based on two steps (see Fig. 2, bottom). Specifically, given a pair of real image and its corresponding segmentation masks (extracted using [4], see Sec. 4.1) (I, I_s), we first generate $\tilde{I}_s = G_{3D}(z_c, z_s, z_p)$ and we optimize $\|\tilde{I}_s - I_s\|_1$ with respect to z_c, z_s and z_p . Let z_c^*, z_s^* and z_p^* be the optimal values so found, and let $\tilde{I}_s^* = G_{3D}(z_c^*, z_s^*, z_p^*)$. Then, we use $\tilde{I} = G_t(\tilde{I}_s^*, z_t)$ and we optimize $\|\tilde{I} - I\|_1 + \tau LPIPS(\tilde{I}, I)$ with respect to z_t , where $LPIPS(I^1, I^2)$ is the $LPIPS$ distance between two images [71] and we use $\tau = 10$.

Once obtained the latent codes ($z_c^*, z_s^*, z_p^*, z_t^*$) corresponding to a real image, editing can be easily done by changing these codes, e.g., using a linear interpolation between codes extracted from different real images.

6. Experiments

Datasets. We evaluate 3D-SGAN on the DeepFashion In-shop Clothes Retrieval benchmark [37], which consists of 52,712 high-resolution person images (1101×750 resolution) with various appearances and poses. This dataset has

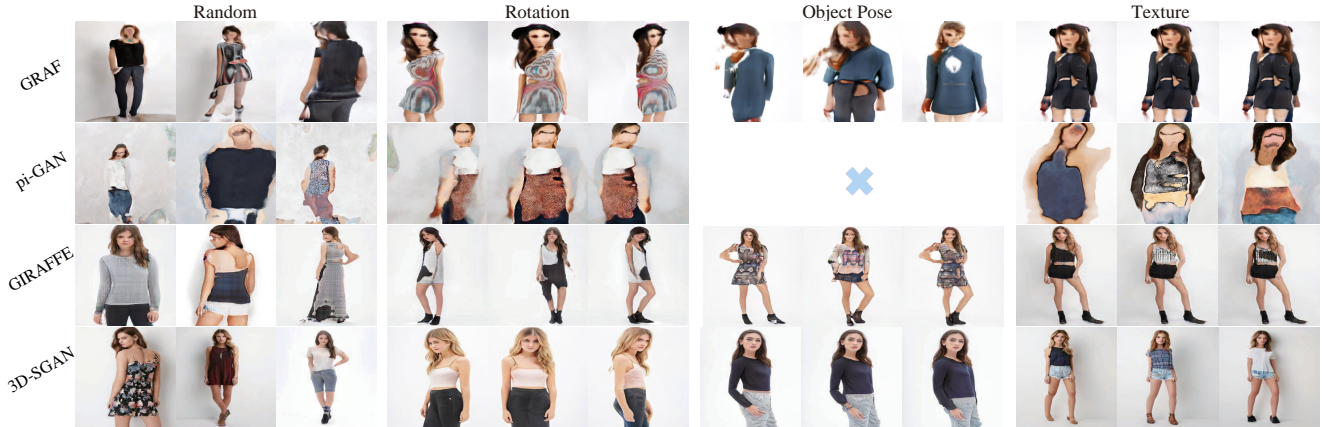


Figure 5: Qualitative comparison. ‘Random’ means that the results are generated by random sampling the latent codes from the corresponding learned marginal distributions. The other 3 columns show controllable person generation with respect to the rotation, the human pose, and the texture attributes. Note that pi-GAN lacks of the results for ‘Object Pose’ because it does not include a latent pose code.

Method	Random	Rotation	Object Pose	Texture
GRAF [60]	52.68	176.9	57.76	220.9
pi-GAN [7]	137.6	213.7	-	135.23
GIRAFFE [49]	42.73	123.4	82.61	98.41
3D-SGAN (ours)	8.240	117.3	54.00	60.63

Table 1: Quantitative comparison using FID scores (\downarrow).

been widely used in pose transfer tasks. We use the following preprocessing. First, we remove overly cropped images, such as incomplete images of humans. Then, the remaining 42,978 images are resized into a 256×256 resolution, and are divided into 41,001 training and 1,976 test images.

Training details. We first train G_t and then we train G_{3D} . Following GIRAFFE [49], the camera distribution P_c can be implemented by first sampling the camera code from a uniform distribution over the dataset-dependent camera elevation angles, and then applying an object affine transformation to sampling 3D points and rays. Both G_t and G_{3D} are trained using the RMSprop optimizer [33]. The learning rate for both the discriminator and the generator is set to 10^{-4} . For the loss weights, we use: $\lambda_1=0.01$, $\lambda_2=0.01$, $\lambda_3=1$, and $\lambda_4=1$. For GAN inversion, we use the Adam optimizer [31] with a learning rate of 10^{-2} . More details are included in the appendix.

Baselines. We compare 3D-SGAN with three state-of-the-art 3D-aware generative approaches, i.e., GRAF [60], pi-GAN [7] and GIRAFFE [49]. For each baseline, we use the corresponding publicly available code with minor adaptations for the DeepFashion dataset. For a fair comparison, we train all the methods on the DeepFashion dataset.

6.1. Comparisons with state-of-the-art methods

Unconditioned human generation. Fig. 5 (“Random” column) shows a qualitative comparison between image sam-

ples generated by all the models. Both GRAF [60] and pi-GAN [7] fail to generate realistic human images. On the other hand, GIRAFFE [49] generates very reasonable human images, but it still suffers from visual artifacts and texture blurs. Compared with these baselines, 3D-SGAN synthesizes much better and more photo-realistic results.

In the first column of Table 1 we provide a quantitative evaluation using FID [20] scores, which are computed using 5,000 randomly sampled images, following standard practice. We observe that 3D-SGAN significantly outperforms all the other baselines, quantitatively confirming the qualitative analysis in Fig. 5.

Controllable human generation. We analyse the representation controllability of all the models. The representation controllability reflects the ability of a model to disentangle different attributes from each other. We achieve this by manipulating a single latent code while fixing the others.

Fig. 5 (columns “Rotation”, “Object Pose” and “Texture”) shows a qualitative comparison by varying only a single latent code. We observe that all the models can rotate the camera viewpoint. However, GRAF [60] fails to disentangle object pose and texture, showing that for GRAF [60] it is hard to model complex pose variations. Moreover, pi-GAN [7] also suffers from the same problem, since it uses one single latent code to model both texture and pose.

On the other hand, both GIRAFFE [49] and 3D-SGAN can effectively disentangle the different variation factors. However, GIRAFFE [49] suffers from multi-view inconsistencies and mode collapse for texture generation. Compared with the baselines, our model has a better view consistency and a more realistic generation. Table 1 quantitatively confirms of the aforementioned observations.

Fig. 6 shows additional controllable human image generation results obtained with 3D-SGAN. The generated im-



Figure 6: Controllable person generation by interpolating latent codes (Rows 1-4). The 5-th row shows texture generation results obtained randomly sampling z_t .

Variants	w/o ℓ_{ss}	w/ ℓ_{ss}
L1↓	5.2489	3.9614

Table 2: A quantitative analysis of the silhouette consistency loss.

ages are realistic and, most of the time, the attributes are effectively disentangled. Specifically, Fig. 6 (1-st row) shows camera rotation results. The images generated by interpolating the camera pose parameter are consistent, and the transition from one image to the next is smooth, while simultaneously preserving the other attributes such as the texture and the pose. On the other hand, Fig. 6 (2-nd row) shows images generated by interpolating the pose code. We again observe that human identity has been well preserved. Additionally, Fig. 6 (3-rd row) shows that the head poses from left to right have slight changes. i.e., face frontalization. It can be explained that the limited training data and the special distribution of fashion images give rise to data bias.

6.2. Ablation study

The consistency losses. Fig. 7 (a) shows a comparison between the results generated by 3D-SGAN with and without ℓ_{ss} . The effectiveness of ℓ_{ss} is shown by observing that, when removed, the generation process suffers from serious geometric inconsistencies. Specifically, the segmentation masks in Fig. 7 (a1) have undesirable pose variations, while Fig. 7 (a2) shows that ℓ_{ss} can largely alleviate this problem. To quantitatively evaluate this effect, we randomly

sample two different semantic codes and we compute the $L1$ distance between the silhouettes of the corresponding generated segmentations. We average the scores over 500 different samples. The result is reported in Tab. 2, which quantitatively validates the effectiveness of this loss for improving the geometric consistency.

Analogously, Fig. 7 (b) shows a comparison between 3D-SGAN generations obtained with and without ℓ_{ps} . This qualitative analysis shows that ℓ_{ps} improves the semantic consistency with respect to different pose codes. For instance, Fig. 7 (b1) shows that there is no “red” region in the segmentation masks in the 1-st and the 2-nd column. However, this region is present in the 3-rd and in the 4-th columns. Conversely, Fig. 7 (a2) shows that ℓ_{ps} can alleviate this phenomenon.

The 3D generator. In our method, we use a GNeRF approach to implicitly represent 3D information. To verify the benefit of using a GNeRF based generator, we replace it with a vanilla GAN (G_{2D}), which takes the pose and the semantics code as inputs. In this experiment, we keep all the other modules fixed. Clearly, G_{2D} lacks the camera parameters and cannot generate images from multiple viewpoints. Moreover, G_{3D} can better disentangle the semantic and the pose factors with respect to G_{2D} , as demonstrated by Fig. 7 (c), where we show interpolation results between two different semantics codes.

The semantic masks and the texture generator. Existing methods such as GRAF [60] and GIRAFFE [49] do not use an additional texture generator which translates seman-

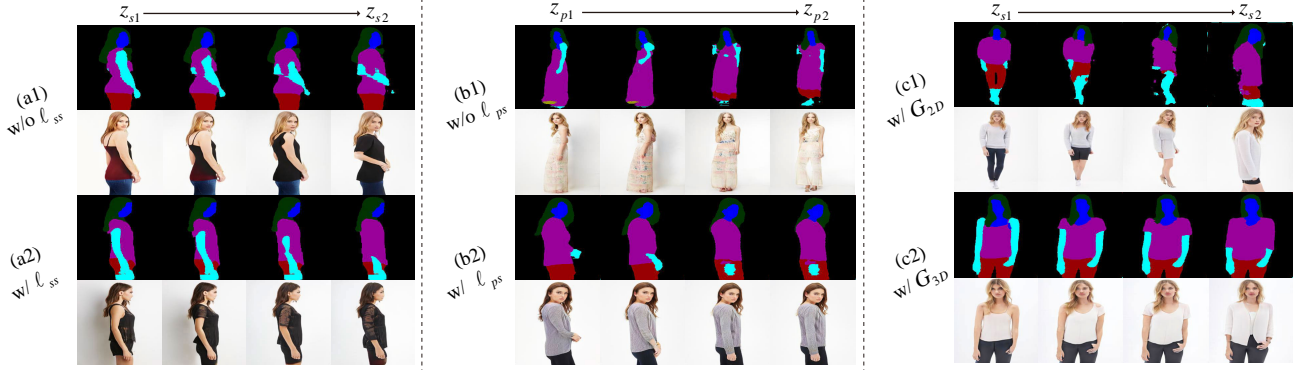


Figure 7: A qualitative analysis of the silhouette-based geometric consistency loss ℓ_{ss} (a), the pose-based semantic consistency loss ℓ_{ps} (b), and the 3D generator G_{3D} (c). (a) and (c) show interpolation results between semantics codes z_{s1} and z_{s2} . (b) shows interpolation results between pose codes z_{p1} and z_{p2} . G_{2D} means G_{3D} where the GNeRF architecture is replaced with a vanilla GAN.



Figure 8: An analysis of the impact of the semantic masks (a) and the VAE-conditioned texture generator (b).

tic masks into textured images. In contrast, the effectiveness of our semantic-based approach is shown in Fig. 5 and Table 1. However, to provide an apple-to-apple comparison and further verify the effectiveness of the semantic masks, we use an additional baseline. Specifically, in this baseline, we render the 3D representation of G_{3D} into features rather than semantic masks and we use the texture generator to map these features into the final image. Fig. 8 (a) shows the comparison of our full model with this baseline. We observe that the baseline (w/o semantic masks) fails to generate high-quality human images. Moreover, our model outperforms this baseline quantitatively in terms of FID scores.

The Variational Autoencoder. We evaluate the effect of conditioning G_t using a VAE (Sec. 4.2). This is done by removing the texture encoder E_t jointly with ℓ_{kl} and ℓ_r from Eq. (10). Fig. 8 (b) shows the comparison between the VAE-based approach and this variant. Both models generate human images with a high texture variability. However, the variant w/o VAE fails to preserve semantic information, i.e., the coherence between the semantic masks, describing the clothes layout, and the final generated clothes. This shows that our VAE-based G_t learns to effectively map the semantic tensors to human images while modeling the texture distribution with the latent code z_t .

6.3. Real human image editing

In this section, we use GAN inversion for real data editing tasks (see Sec. 5). The 2-nd column of Fig. 9 shows that the optimal latent code values (z_c^* , z_s^* , z_p^* , z_t^*), obtained using the procedure described in Sec. 5, lead to an effective reconstruction of the real input data (1-st column). In other columns, we linearly manipulate the semantic code z_s^* , while keeping fixed the other codes. Specifically, the second row of Fig. 9 shows the photo-realistic final images corresponding to the semantic masks in the first row. These results demonstrates the effectiveness of the GAN inversion mechanism and the possibility to apply our model to a wide range of human image editing tasks.

7. Conclusion

We propose a novel 3D-aware Semantic-Guided Generative model (3D-SGAN) for human synthesis. Specifically, we use a generative NeRF to implicitly represent the 3D human body and render 3D representation into 2D semantic masks. Then, the semantic masks are mapped into the final photo-realistic images using a VAE-conditioned texture generator. Moreover, we propose two consistency losses further to disentangle the geometry pose and the semantics factors. Our experiments show that the proposed approach

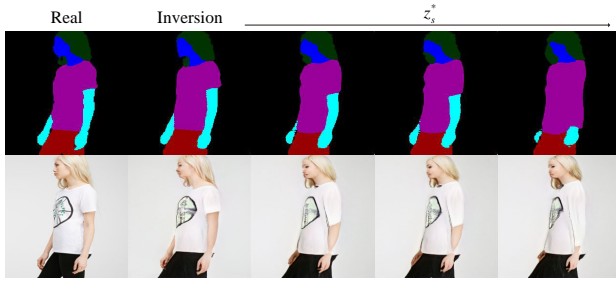


Figure 9: Real data semantic editing results using GAN inversion. The optimal semantic code z_s^* , searching by GAN inversion, can be manipulated to achieve human semantic editing.

generates human images which are more realistic and more controllable than state-of-the-art methods.

Limitations. The results from our model are not always perfect, such as low-quality generation and unqualified disentanglement in some cases. As for the reasons, the limited training data and the special distribution of fashion data give rise to data bias and make the model struggle sometimes to disentangle the multiple factors in human person generation. Additionally, the GAN inversion method that we use compromises the reconstruction and the editing ability. A more effective disentanglement and GAN inversion method will be explored in the future.

Potential Negative Impact. Despite the wide interesting applications of real data editing, it may give rise to the infringement of people’s privacy. Therefore, the governments and the developers should establish strict laws and regulations to avoid the negative impact that the human editing task may cause.

References

- [1] Rameen Abdal, Yipeng Qin, and Peter Wonka. Image2stylegan: How to embed images into the stylegan latent space? In *ICCV*, 2019. 5
- [2] Rameen Abdal, Peihao Zhu, Niloy Mitra, and Peter Wonka. Styleflow: Attribute-conditioned exploration of stylegan-generated images using conditional continuous normalizing flows. *ACM TOG*, 2020. 1
- [3] Rıza Alp Güler, Natalia Neverova, and Iasonas Kokkinos. Densepose: Dense human pose estimation in the wild. In *CVPR*, 2018. 2
- [4] Vijay Badrinarayanan, Alex Kendall, and R. Cipolla. Segnet: A deep convolutional encoder-decoder architecture for image segmentation. *IEEE TPAMI*, 39, 2017. 4, 5
- [5] G. Balakrishnan, Amy Zhao, Adrian V. Dalca, F. Durand, and J. Guttag. Synthesizing images of humans in unseen poses. In *CVPR*, 2018. 3
- [6] Andrew Brock, Jeff Donahue, and Karen Simonyan. Large scale gan training for high fidelity natural image synthesis. In *ICLR*, 2019. 2
- [7] Eric Chan, Marco Monteiro, Petr Kellnhofer, Jiajun Wu, and Gordon Wetzstein. pi-gan: Periodic implicit generative adversarial networks for 3d-aware image synthesis. In *arXiv*, 2020. 1, 6
- [8] Xuelin Chen, Daniel Cohen-Or, Baoquan Chen, and Niloy Jyoti Mitra. Towards a neural graphics pipeline for controllable image generation. *CGF*, 2021. 1, 2
- [9] Yunjey Choi, Minje Choi, Munyoung Kim, Jung-Woo Ha, Sunghun Kim, and Jaegul Choo. Stargan: Unified generative adversarial networks for multi-domain image-to-image translation. In *CVPR*, 2018. 1
- [10] Terrance DeVries, Miguel Angel Bautista, Nitish Srivastava, Graham W. Taylor, and Joshua M. Susskind. Unconstrained scene generation with locally conditioned radiance fields. In *ICCV*, 2021. 1, 2
- [11] Matheus Gadelha, Subhransu Maji, and Rui Wang. 3d shape induction from 2d views of multiple objects. In *3DV*, 2017. 1, 2
- [12] Ian Goodfellow, Jean Pouget-Abadie, Mehdi Mirza, Bing Xu, David Warde-Farley, Sherjil Ozair, Aaron Courville, and Yoshua Bengio. Generative adversarial nets. In *NeurIPS*, 2014. 1, 2
- [13] Artur Grigorev, Karim Iskakov, Anastasia Ianina, Renat Bashirov, Ilya Zakharkin, Alexander Vakhitov, and Victor Lempitsky. Stylepeople: A generative model of fullbody human avatars. In *CVPR*, 2021. 3
- [14] A. Grigorev, A. Sevastopolsky, Alexander Vakhitov, and V. Lempitsky. Coordinate-based texture inpainting for pose-guided image generation. In *CVPR*, 2019. 3
- [15] Rıza Alp Güler, Natalia Neverova, and Iasonas Kokkinos. Densepose: Dense human pose estimation in the wild. In *CVPR*, 2018. 3
- [16] Ishaan Gulrajani, Faruk Ahmed, Martin Arjovsky, Vincent Dumoulin, and Aaron Courville. Improved training of wasserstein gans. In *NeurIPS*, 2017. 1
- [17] Zhenliang He, Meina Kan, and Shiguang Shan. Eigengan: Layer-wise eigen-learning for gans. In *ICCV*, 2021. 1
- [18] Paul Henderson and Vittorio Ferrari. Learning single-image 3d reconstruction by generative modelling of shape, pose and shading. *IJCV*, 2019. 2
- [19] Philipp Henzler, Niloy J. Mitra, and Tobias Ritschel. Escaping plato’s cave: 3d shape from adversarial rendering. In *ICCV*, 2019. 2
- [20] Martin Heusel, Hubert Ramsauer, Thomas Unterthiner, Bernhard Nessler, and Sepp Hochreiter. Gans trained by a two time-scale update rule converge to a local nash equilibrium. In *NeurIPS*, 2017. 6
- [21] Siyu Huang, Haoyi Xiong, Zhi-Qi Cheng, Qingzhong Wang, Xingran Zhou, Bihan Wen, Jun Huan, and Dejing Dou. Generating person images with appearance-aware pose stylizer. In *IJCAI*, 2020. 3
- [22] Xun Huang, Ming-Yu Liu, Serge Belongie, and Jan Kautz. Multimodal unsupervised image-to-image translation. In *ECCV*, 2018. 1
- [23] Ajay Jain, Matthew Tancik, and Pieter Abbeel. Putting nerf on a diet: Semantically consistent few-shot view synthesis. In *ICCV*, 2021. 1

- [24] Zhang Jinsong, Li Kun, Lai Yu-Kun, and Yang Jingyu. PISE: Person image synthesis and editing with decoupled gan. In *CVPR*, 2021. 3
- [25] Tero Karras, Timo Aila, Samuli Laine, and Jaakko Lehtinen. Progressive growing of gans for improved quality, stability, and variation. In *ICLR*, 2018. 1, 2
- [26] Tero Karras, Miika Aittala, Janne Hellsten, Samuli Laine, Jaakko Lehtinen, and Timo Aila. Training generative adversarial networks with limited data. In *NeurIPS*, 2020. 1
- [27] Tero Karras, Miika Aittala, Samuli Laine, Erik Härkönen, Janne Hellsten, Jaakko Lehtinen, and Timo Aila. Alias-free generative adversarial networks. In *NeurIPS*, 2021. 1
- [28] Tero Karras, Samuli Laine, and Timo Aila. A style-based generator architecture for generative adversarial networks. In *CVPR*, 2019. 1, 2
- [29] Tero Karras, Samuli Laine, Miika Aittala, Janne Hellsten, Jaakko Lehtinen, and Timo Aila. Analyzing and improving the image quality of stylegan. In *CVPR*, 2020. 1, 2, 3, 4
- [30] Tero Karras, S. Laine, Miika Aittala, Janne Hellsten, J. Lehtinen, and Timo Aila. Analyzing and improving the image quality of stylegan. In *CVPR*, 2020. 2
- [31] Diederik P. Kingma and Jimmy Ba. Adam: A method for stochastic optimization. In *ICLR*, 2015. 6
- [32] Diederik P Kingma and Max Welling. Auto-encoding variational bayes. *arXiv preprint arXiv:1312.6114*, 2013. 2, 4
- [33] Diederik P. Kingma and Max Welling. Auto-encoding variational bayes. In *ICLR*, 2013. 6
- [34] Anders Boesen Lindbo Larsen, Søren Kaae Sønderby, Hugo Larochelle, and Ole Winther. Autoencoding beyond pixels using a learned similarity metric. In *ICML*, 2016. 5
- [35] Yiyi Liao, Katja Schwarz, Lars Mescheder, and Andreas Geiger. Towards unsupervised learning of generative models for 3d controllable image synthesis. In *CVPR*, 2020. 1, 2
- [36] Wen Liu, Zhixin Piao, Zhi Tu, Wenhan Luo, Lin Ma, and Shenghua Gao. Liquid warping gan with attention: A unified framework for human image synthesis. *IEEE TPAMI*, 2021. 3
- [37] Ziwei Liu, Ping Luo, Shi Qiu, Xiaogang Wang, and Xiaoou Tang. Deepfashion: Powering robust clothes recognition and retrieval with rich annotations. In *CVPR*, 2016. 2, 5
- [38] Matthew Loper, Naureen Mahmood, Javier Romero, Gerard Pons-Moll, and Michael J. Black. SMPL: A skinned multi-person linear model. *ACM TOG*, 2015. 3
- [39] Sebastian Lunz, Yingzhen Li, Andrew W. Fitzgibbon, and Nate Kushman. Inverse graphics GAN: learning to generate 3d shapes from unstructured 2d data. *CoRR*, abs/2002.12674, 2020. 2
- [40] Zhengyao Lv, Xiaoming Li, Xin Li, Fu Li, Tianwei Lin, Dongliang He, and Wangmeng Zuo. Learning semantic person image generation by region-adaptive normalization. In *CVPR*, 2021. 3
- [41] Liqian Ma, Xu Jia, Qianru Sun, Bernt Schiele, Tinne Tuytelaars, and Luc Van Gool. Pose guided person image generation. In *NeurIPS*, 2017. 3
- [42] Liqian Ma, Qianru Sun, Stamatios Georgoulis, Luc Van Gool, Bernt Schiele, and Mario Fritz. Disentangled person image generation. In *CVPR*, 2018. 3
- [43] Yifang Men, Yiming Mao, Yuning Jiang, Wei-Ying Ma, and Zhouhui Lian. Controllable person image synthesis with attribute-decomposed gan. In *CVPR*, 2020. 3
- [44] Ben Mildenhall, Pratul P. Srinivasan, Matthew Tancik, Jonathan T. Barron, Ravi Ramamoorthi, and Ren Ng. Nerf: Representing scenes as neural radiance fields for view synthesis. In *ECCV*, 2020. 1, 3, 4
- [45] Natalia Neverova, Riza Alp Guler, and Iasonas Kokkinos. Dense pose transfer. In *ECCV*, 2018. 3
- [46] Thu Nguyen-Phuoc, Chuan Li, Lucas Theis, Christian Richardt, and Yong-Liang Yang. Hologan: Unsupervised learning of 3d representations from natural images. In *ICCV*, 2019. 1, 2
- [47] Thu Nguyen-Phuoc, Christian Richardt, Long Mai, Yong-Liang Yang, and Niloy Mitra. Blockgan: Learning 3d object-aware scene representations from unlabelled images. In *NeurIPS*, 2020. 1, 2
- [48] Michael Niemeyer and Andreas Geiger. CAMPARI: camera-aware decomposed generative neural radiance fields. In *3DV*, 2021. 2
- [49] Michael Niemeyer and Andreas Geiger. GIRAFFE: Representing scenes as compositional generative neural feature fields. In *CVPR*, 2021. 1, 2, 3, 4, 6, 7
- [50] Taesung Park, Ming-Yu Liu, Ting-Chun Wang, and Jun-Yan Zhu. Semantic image synthesis with spatially-adaptive normalization. In *CVPR*, 2019. 1
- [51] Sida Peng, Junting Dong, Qianqian Wang, Shangzhan Zhang, Qing Shuai, Hujun Bao, and Xiaowei Zhou. Animatable neural radiance fields for human body modeling. In *ICCV*, 2021. 1
- [52] Sida Peng, Yuanqing Zhang, Yinghao Xu, Qianqian Wang, Qing Shuai, Hujun Bao, and Xiaowei Zhou. Neural body: Implicit neural representations with structured latent codes for novel view synthesis of dynamic humans. In *CVPR*, 2021. 1
- [53] Christian Reiser, Songyou Peng, Yiyi Liao, and Andreas Geiger. Kilonerf: Speeding up neural radiance fields with thousands of tiny mlps. In *ICCV*, 2021. 1
- [54] Yurui Ren, Xiaoming Yu, Junming Chen, Thomas H Li, and Ge Li. Deep image spatial transformation for person image generation. In *CVPR*, 2020. 3
- [55] Danilo Jimenez Rezende, S. M. Ali Eslami, Shakir Mohamed, Peter Battaglia, Max Jaderberg, and Nicolas Heess. Unsupervised learning of 3d structure from images. In *NeurIPS*, 2016. 2
- [56] Soubhik Sanyal, Alex Vorobiov, Timo Bolkart, Matthew Loper, Betty Mohler, Larry S. Davis, Javier Romero, and Michael J. Black. Learning realistic human reposing using cyclic self-supervision with 3d shape, pose, and appearance consistency. In *ICCV*, 2021. 3
- [57] Kripasindhu Sarkar, Vladislav Golyanik, Lingjie Liu, and Christian Theobalt. Style and pose control for image synthesis of humans from a single monocular view. *arXiv preprint arXiv:2102.11263*, 2021. 3
- [58] Kripasindhu Sarkar, Lingjie Liu, Vladislav Golyanik, and Christian Theobalt. Humangan: A generative model of humans images. *arXiv preprint arXiv:2103.06902*, 2021. 2, 3

- [59] Kripasindhu Sarkar, Dushyant Mehta, Weipeng Xu, Vladislav Golyanik, and Christian Theobalt. Neural re-rendering of humans from a single image. In *ECCV*, 2020. 3
- [60] Katja Schwarz, Yiyi Liao, Michael Niemeyer, and Andreas Geiger. Graf: Generative radiance fields for 3d-aware image synthesis. In *NeurIPS*, 2020. 1, 2, 3, 4, 6, 7
- [61] Yujun Shen, Jinjin Gu, Xiaoou Tang, and Bolei Zhou. Interpreting the latent space of gans for semantic face editing. In *CVPR*, 2020. 1
- [62] Yujun Shen and Bolei Zhou. Closed-form factorization of latent semantics in gans. In *CVPR*, 2021. 1
- [63] Aliaksandr Siarohin, Stéphane Lathuilière, Enver Sangineto, and Nicu Sebe. Appearance and Pose-Conditioned Human Image Generation using Deformable GANs. *IEEE TPAMI*, 2020. 3
- [64] Aliaksandr Siarohin, Stéphane Lathuilière, Sergey Tulyakov, Elisa Ricci, and Nicu Sebe. First order motion model for image animation. In *NeurIPS*, 2019. 3
- [65] Hao Tang, Song Bai, Philip HS Torr, and Nicu Sebe. Bipartite graph reasoning gans for person image generation. In *BMVC*, 2020. 3
- [66] Hao Tang, Song Bai, Li Zhang, Philip HS Torr, and Nicu Sebe. Xinggan for person image generation. In *ECCV*, 2020. 3
- [67] Omer Tov, Yuval Alaluf, Yotam Nitzan, Or Patashnik, and Daniel Cohen-Or. Designing an encoder for stylegan image manipulation. *ACM TOG*, 2021. 1
- [68] X. Wang and Abhinav Gupta. Generative image modeling using style and structure adversarial networks. In *ECCV*, 2016. 2
- [69] Jiajun Wu, Chengkai Zhang, Tianfan Xue, William T Freeman, and Joshua B Tenenbaum. Learning a probabilistic latent space of object shapes via 3d generative-adversarial modeling. In *NeurIPS*, 2016. 1, 2
- [70] Jichao Zhang, Aliaksandr Siarohin, Hao Tang, Jingjing Chen, Enver Sangineto, Wei Wang, and Nicu Sebe. Controllable person image synthesis with spatially-adaptive warped normalization. *Arxiv*, 2021. 3
- [71] Richard Zhang, Phillip Isola, Alexei A Efros, Eli Shechtman, and Oliver Wang. The unreasonable effectiveness of deep features as a perceptual metric. In *CVPR*, 2018. 5
- [72] Xingran Zhou, Bo Zhang, Ting Zhang, Pan Zhang, Jianmin Bao, Dong Chen, Zhongfei Zhang, and Fang Wen. Cocosnet v2: Full-resolution correspondence learning for image translation. In *CVPR*, 2021. 3
- [73] Jun-Yan Zhu, Taesung Park, Phillip Isola, and Alexei A Efros. Unpaired image-to-image translation using cycle-consistent adversarial networks. In *ICCV*, 2017. 1
- [74] Jun-Yan Zhu, Zhoutong Zhang, Chengkai Zhang, Jiajun Wu, Antonio Torralba, Joshua B. Tenenbaum, and William T. Freeman. Visual object networks: Image generation with disentangled 3D representations. In *NeurIPS*, 2018. 1, 2
- [75] Zhen Zhu, Tengteng Huang, Baoguang Shi, Miao Yu, Bofei Wang, and Xiang Bai. Progressive pose attention transfer for person image generation. In *CVPR*, 2019. 3